Chemical and Heisenberg Exchange in Ion-Pair Solutions Revisited by Two-Dimensional EPR Spectroscopy

S. Kababya, Z. Luz, and D. Goldfarb*

Contribution from the Chemical Physics Department, Weizmann Institute of Science, 76 100 Rehovot, Israel

*Received December 6, 1993**

Abstract: The dynamic processes in tetrahydrofuran (THF) solutions of 2,5-di-*tert*-butyl-*p*-benzoquinone$^-$, Na^+ (DtBPBQ$^-$, Na^+) ion-pairs, obtained by reduction with a sodium mirror, have been studied by two-dimensional (2D) exchange Fourier transform (FT) EPR spectroscopy. Measurements were made at room temperature (17–20 °C) on solutions with radical concentrations ranging from 4.5×10^{-5} to 3.5×10^{-3} M and with mixing times varying from 0.3 to 6 μs. Analysis of the EPR spectra indicates the presence of two types of DtBPBQ$^-$, Na^+ ion-pairs, which are labeled A and B. In both species there is intramolecular Na^+ hopping, but while in ion-pair A the process is slow and suitable for monitoring by the 2D exchange method, in ion-pair B it is much faster and results in a selective smearing of some of the hyperfine lines. The origin of the latter is tentatively ascribed to complexation with OH^- generated by water impurity. In the 2D spectra characteristic cross peaks due to Na^+ hopping and Heisenberg exchange (HE) appear. Analysis of these spectra provides information about the intramolecular Na^+ hopping rate in ion-pair A, k_{CE}^A, as well as on the HE rate constants, k_{ll}, of the various radicals. At room temperature these are $k_{CE}^A = (1.7 \pm 0.2) \times 10^5\ s^{-1}$, $k_{AA} = (7.5 \pm 1.0) \times 10^8\ s^{-1}\ mol^{-1}$, and $k_{BB} = (1.0 \pm 0.2) \times 10^8\ s^{-1}\ mol^{-1}$. These results also provide information on the longitudinal relaxation rates of the overall magnetization of both radicals. These depend on the total radical concentration and within experimental accuracy are the same for both radicals. The mechanism for this process is tentatively ascribed to electron–electron (radical–radical) dipolar interaction, and its rate is compared with calculations based on the point dipole approximation. The present work demonstrates the power of the 2D exchange EPR method in elucidating mechanisms of dynamic processes and determining kinetic parameters, in particular when several such processes occur simultaneously.

Introduction

Electron paramagnetic resonance (EPR) spectroscopy is an invaluable technique for the investigation of rates and mechanisms of chemical reactions involving paramagnetic compounds. Generally, reactions with rates in the range 10^5–$10^{10}\ s^{-1}$ are well suited for EPR investigations either by line-shape analysis or through relaxation measurements. A specific area that has been extensively studied by dynamic EPR is that of radical ion-pairs,[1] including for example interconversion between tight and loosely bound pairs, structural changes within ion-pairs, intramolecular cation migration, and cation exchange.[1,2] In addition to rate constants, reaction mechanism, and thermodynamic parameters, such studies also yield information concerning the structure of the ion-pair and on solvation effects.[1-4]

In the slow exchange limit where the reaction rate is on the order of, or smaller than, the natural line width, line-shape analysis of continuous wave (CW) EPR spectra is no longer applicable. Under these conditions one has to rely on small line-width changes, which may also arise from other line-broadening mechanisms, in particular, Heisenberg exchange. Attempts to extend the range of exchange rates that can be measured by EPR methods to lower rates were made using electron-nuclear double resonance (ENDOR) spectroscopy.[5,6] In this method one takes advantage of the narrower ENDOR lines and of the variation of their intensities arising from changes in the saturation behavior of different hyperfine lines due to chemical exchange. An analysis of the latter is, however, complicated by the complex dependence of the ENDOR peak intensities on the relaxation mechanisms.[5]

A simpler alternative way to extend the "dynamic" range of EPR spectroscopy is to apply the two-dimensional (2D) exchange Fourier transform (FT) method. The method is the microwave analog of the 2D exchange NMR spectroscopy of Jeener et al.[7] In this experiment the range of exchange rates that can be measured is limited by the spin lattice relaxation time, T_1, rather than by the, usually shorter, transverse relaxation time. The recent technological developments of fast digitizers and new microwave components allow pulse experiments, similar to those developed for NMR, to be carried out in the EPR regime. Several 2D FT-EPR experiments have already been reported, including measurements of electron transfer[8] and Heisenberg exchange (HE),[9,10] as well as studies of slow reorientational motions[11-13] and nuclear modulation effects.[12] In a previous short communication we showed that 2D exchange EPR can also be used to study slow chemical exchange in radicals.[14] This was specifically demonstrated for the cation hopping in the ion-pair 2,5-*di-tert*-butyl-*p*-benzoquinone$^-$, Na^+ (DtBPBQ$^-$, Na^+) in tetrahydrofuran (THF) solutions.[14] Two-dimensional exchange EPR spectra exhibit cross peaks between hyperfine lines among

* Abstract published in *Advance ACS Abstracts*, May 15, 1994.

(1) Sharp, J. H.; Symons, M. C. R. In *Ions and Ion-Pairs in Organic Reactions*; Szwarc, M., Ed.; Wiley Interscience: New York, 1972; Vol. I, Chapter 5.

(2) Chen, K. S.; Hirota, N. In *Investigation of Rates and Mechanisms of Reactions*, part II; Hammes, G. G., Ed.; Wiley Interscience: New York, 1974; p 565.

(3) Claxton, T. A.; Oakes, J.; Symons, M. C. R. *Trans. Faraday Soc.* **1967**, *63*, 2125.

(4) Symons, M. C. R. *J. Phys. Chem.* **1967**, *71*, 172.

(5) Atherton, N. M.; Kennedy, P. *J. Chem. Soc., Faraday Trans.* **1978**, *74*, 67.

(6) Von Borczyskowski, C.; Möbius, K. *Chem. Phys.* **1976**, *12*, 281.

(7) Jeener, J.; Meier, B. H.; Bachmann, P.; Ernst, R. R. *J. Chem. Phys.* **1979**, *71*, 4546.

(8) Angerhofer, A.; Massoth, R. J.; Bowman, M. K. *Isr. J. Chem.* **1988**, *28*, 227.

(9) (a) Gorcester, J.; Freed, J. H. *J. Chem. Phys.* **1986**, *85*, 5375. (b) Gorcester, J.; Freed, J. H. *J. Chem. Phys.* **1988**, *88*, 4678.

(10) Gorcester, J.; Rananavare, S.; Freed, J. H. *J. Chem. Phys.* **1989**, *96*, 5764.

(11) Patyal, B. R.; Crepeau, R. H.; Gamliel, D.; Freed, J. H. *Chem. Phys. Lett.* **1990**, *175*, 445.

(12) Lee, S.; Patyal, B. R.; Freed, J. H. *J. Chem. Phys.* **1993**, *98*, 3665.

(13) Patyal, B. R.; Crepeau, R. H.; Gamliel, D.; Freed, J. H. *J. Chem. Phys.* **1990**, *175*, 453.

(14) Fauth, J. M.; Kababya, S.; Goldfarb, D. *J. Magn. Reson.* **1991**, *92*, 203.

0002-7863/94/1516-5805$04.50/0

Scheme 1

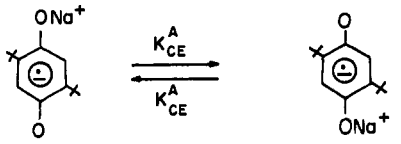

which magnetization transfer takes place during a preset mixing time.[8-10,14] While magnetization transfer generated by bimolecular processes such as HE or electron transfer yields cross peaks between all hyperfine lines in the spectrum,[8,9] chemical exchange results in a cross peak pattern which is characteristic of the particular reaction mechanism.[14,15]

When chemical exchange (CE) processes are studied by the CW EPR methods, it is desirable to work with dilute samples, thus minimizing electron transfer and HE processes whose presence may complicate the determination of the CE rates.[16] It is sometimes, however, not possible to control the radical formation to a degree that fully eliminates these processes. With the 2D methods it is not only possible to accurately determine the chemical exchange rate but it can be done in the presence of other processes, the rates of which can simultaneously be obtained.

In the present work we extend our previous study on the intramolecular cation migration in the DtBPBQ$^-$, Na$^+$–THF system (Scheme 1). Earlier CW EPR measurements on this system by Warhurst et al.[17] and by Hirota et al.[2] gave quite different exchange rates for the process, and we hope to clarify the discrepancy using the 2D exchange method. The room temperature (RT) CW EPR spectrum of this system is characteristic of an asymmetric ion-pair. It consists of four peaks due to hyperfine interaction with two inequivalent aromatic protons. When the intramolecular ion hopping is fast, as in the case of the corresponding potassium ion-pair, the temperature dependence of the EPR spectrum exhibits the well-known "linewidth alternation effect,"[16] whereby only part of the peaks are affected by the dynamic process.[17-20] Accordingly, in the slow exchange limit, where only minor changes in the line width occur, as in the sodium ion-pair, the process is manifested in the 2D exchange spectra by the appearance of cross peaks only between the two inner hyperfine lines.[14] In the present study a series of samples with varying radical concentrations were investigated and the 2D maps were analyzed in terms of the rates of the CE, HE, and the spin lattice relaxation. The latter two processes are related to the bimolecular collisions of the radicals in the solutions.

Basic Equations. The general pulse sequence employed in 2D exchange spectroscopy is[7] $(\pi/2)_{\varphi 1}-t_1-(\pi/2)_{\varphi 2}-\tau_m-(\pi/2)_{\varphi 3}-t_2$, where the phases φ_1, φ_2, and φ_3 depend on the particular phase cycle employed. The measured 2D signal, under the assumption of slow exchange is given by[21]

$$S(t_1,\tau_m,t_2) = \sum_{i,j} s_{ij}(t_1,\tau_m,t_2) = \sum_{i,j} P_j(0)\, A_{ij}(\tau_m) e^{(i w_j - 1/T_{2j})t_1} e^{(i w_i - 1/T_{2i})t_2} \quad (1)$$

where terms due to axial peaks which are eliminated by the phase cycling have not been included. In eq 1, t_1, τ_m, and t_2 are the pulse sequence time intervals and the indices i, j run over all hyperfine lines. The term $s_{ij}(t_1, \tau_m, t_2)$ corresponds to the intensity of cross peaks when $i \neq j$ and to diagonal peaks when $i = j$, $P_j(0)$ is the relative intensity of the jth hyperfine line, and $A_{ij}(\tau_m)$ is the so-called mixing coefficient and is given by

$$A_{ij}(\tau_m) = e^{\mathbf{R}\tau_m} = \sum_k D_{ik} e^{\Lambda_{kk}\tau_m} D_{kj}^{-1} \quad (2)$$

where $\mathbf{R}$ is the exchange matrix, Λ the diagonal matrix of its eigenvalues, and $\mathbf{D}$ the matrix of its corresponding eigenvectors. After the two-dimensional Fourier transformation the intensity of the (ij) peak is proportional to $A_{ij}(\tau_m)$. By following the peaks' intensiy as a function of the mixing time, the elements of $\mathbf{R}$, which depend on the T_1 and the rates of the CE and HE processes, can be determined.[22] In the case of a two-site exchange (A $\rightleftarrows$ B) with equal concentrations and spin lattice relaxation times, the mixing coefficients become[21]

$$A_{AA}(\tau_m) = A_{BB}(\tau_m) = (1/2)\,(1 + e^{-2K\tau_m}) e^{-\tau_m/T_1}$$

$$A_{AB}(\tau_m) = A_{BA}(\tau_m) = (1/2)(1 - e^{-2K\tau_m}) e^{-\tau_m/T_1} \quad (3)$$

where K is the rate constant for the reaction.

Table 1. Concentration of the DtBPBQ Solutions Studied and of the Ion-Pair, after Reduction with a Sodium Mirror

sample no.	DtBPBQ [M]	DtBPBQ$^-$, Na$^+$ [a] [M]
1	4.5×10^{-5}	4.0×10^{-5}
2	2.3×10^{-4}	2.3×10^{-4}
3	7.9×10^{-4}	4.6×10^{-4} [b]
4	9.0×10^{-4}	6.9×10^{-4}
5	1.2×10^{-3}	1.6×10^{-3}
6	3.4×10^{-3}	1.1×10^{-3} [b]

[a] Determined by a comparison with a series of standard solutions. [b] These solutions were measured a few days after preparation. This may be the cause for the somewhat reduced value compared to the initial concentration of DtBPBQ.

Experimental Section

Sample Preparation. Solutions of DtBPBQ$^-$, Na$^+$ were prepared in a vacuum manifold, using a glass apparatus consisting of two parts. One part contained a reducing sodium mirror and the other, separated by a break seal, a solution of DtBPBQ in THF.[23] The 2D measurements were performed within 1 day after the sample preparation. The total concentrations of the solution, determined from the weight of the quinone and the THF volume, are listed in Table 1. Under the assumption that immediately after reduction the ion-pair yield is 100%, we took the total radical concentration to be equal to the DtBPBQ concentration. This was confirmed by comparing the intensity of the CW EPR spectra with those of standard solutions containing varying concentrations of a stable nitroxide radical (4-hydroxy-2,2,6,6-tetramethylpiperidinooxy). The concentrations obtained in this way are listed in Table 1 as well.

UV–Vis Measurements. UV–Vis spectra of the various solutions were recorded using a UV–Visbal HP 8452A photospectrometer. Examples of spectra of a DtBPBQ solution in THF taken before and after reduction with the sodium mirror are shown in Figure 1. Prior to reduction the spectrum consists of two peaks at 272 and 326 nm (trace a). One minute after the initiation of the reaction (the seal break) the solvent turned yellow and an additional line at 420 nm appeared (trace b). The intensity of this line further increased after a few more minutes of contact with the sodium mirror (trace c). We assign the 420-nm peak to the radical anion, in agreement with the UV–vis spectra of other semiquinone anions.[24] For instance, the spectra of the radical anions 2,5-dimethyl-*p*-benzoquinone$^-$, 2,6-dimethyl-*p*-benzoquinone$^-$, *p*-benzoquinone$^-$, and 2-methyl-*p*-benzoquinone$^-$ in MeTHF solutions all exhibit two peaks at around 325–328 and 400–450 nm.

ESR Measurements. CW X-band (9.0 GHz) EPR measurements were performed on a Varian E-12 spectrometer. The 2D FT-EPR measure-

(15) Weber, R. T. Abstract, High Frequency EPR and Electron Spin Echo Spectroscopy Work-shop, Amsterdam, April 1993.
(16) Chippendale, J. C.; Warhurst, E. *Trans. Faraday Soc.* **1968**, *64*, 2332.
(17) Warhurst, E.; Wilde, A. M. *Trans. Faraday Soc.* **1971**, *67*, 605.
(18) Freed, J. H.; Fraenkel, G. K. *J. Chem. Phys.* **1962**, *37*, 1156.
(19) Sullivan, P. D.; Bolton, J. R. *Adv. Magn. Reson.* **1970**, *4*, 39.
(20) de Boer, E.; Mackor, E. L. *J. Am. Chem. Soc.* **1964**, *86*, 1513.
(21) Ernst, R. R.; Bodenhausen, G.; Wokaum, A. *Principles of Nuclear Magnetic Resonance in One and Two Dimensions*; Oxford Science Publications: Oxford, 1987.
(22) Macura, S.; Ernst, R. R. *Mol. Phys.* **1980**, *41*, 95.
(23) McClelland, B. J.; Carter, H. V.; Warhurst, E. *Trans. Faraday Soc.* **1960**, *56*, 343.
(24) Shida, T. *Electronic Absorption Spectra of Radical Ions*; Elsevier Science Publishers: Essex, 1988.

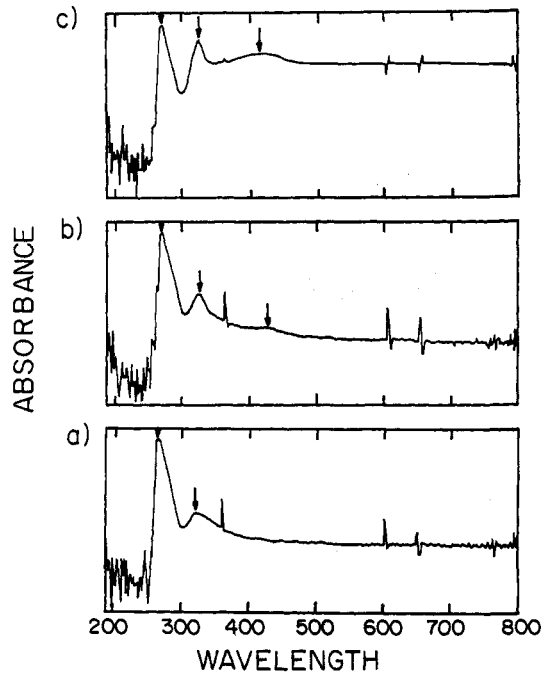

Figure 1. UV–vis spectra of DtBPBQ in THF (solution 4): (a) before reduction with sodium; (b) one minute after reduction initiation; (c) 30 min later. The spikes are instrumental artifacts, and the arrows mark the observed peaks.

Table 2. The Phase Cycle Used[a]

			R	
φ_1	φ_2	φ_3	real	imaginary
X	*X*	*X*	*+a*	*+b*
X	*-X*	*X*	*-a*	*-b*
X	*X*	*-X*	*-a*	*-b*
X	*-X*	*-X*	*+a*	*+b*
X	*X*	*Y*	*+b*	*-a*
X	*-X*	*Y*	*-b*	*+a*
X	*X*	*-Y*	*-b*	*+a*
X	*-X*	*-Y*	*+b*	*-a*
X	*Y*	*Y*	*-a*	*-b*
X	*-Y*	*Y*	*+a*	*+b*
X	*Y*	*-Y*	*+a*	*+b*
X	*-Y*	*-Y*	*-a*	*-b*
X	*Y*	*-X*	*-b*	*+a*
X	*-Y*	*-X*	*+b*	*-a*
X	*Y*	*X*	*+b*	*-a*
X	*-Y*	*X*	*-b*	*+a*

[a] φ_1, φ_2, and φ_3 are the phases of the three pulses, and *R* describes the receiver phase where *a*, *b* are the two quadrature channels which are added to the real or imaginary part of the signal in the computer.

ments were performed at room temperature (17–20 °C) on a home-built spectrometer described elsewhere at ~9.3 GHz.[14,25] The sequence employed was $(\pi/2)_{\varphi_1}$–t_1–$(\pi/2)_{\varphi_2}$–τ_m–$(\pi/2)_{\varphi_3}$–t_2,[7] with a $\pi/2$ pulse width of about 10 ns. As will be seen below, this effectively covered the whole spectral range of the ($DtBPBQ^-$, Na^+) ion pair. The resulting FIDs were collected in quadrature using a 16-step phase cycle, as shown in Table 2, which afforded quadrature detection in t_1 as well. In addition, the phase cycle ensured elimination of axial peaks and quadrature images.[22,26] The 2D spectra are presented in the magnitude mode where we chose to display the "anti echo" signal.[26] This results in a main diagonal stretching from top left to bottom right. The dwell time was 20 ns in both t_1 and t_2 (corresponding to a spectral width of 50 MHz in both dimensions). Seventy points were collected for t_1 and 130 for t_2. Depending on the S/N level, between 500 and 3000 scans were accumulated for each step in the phase cycle. The repetition rate was 100 Hz and the spectrometer deadtime 160 ns. The mixing time varied between 0.3 and 6.0 μs. Spectra

(25) Goldfarb, D.; Fauth, J. M.; Tor, Y.; Shanzer, A. *J. Am. Chem. Soc.* **1991**, *113*, 1941.

(26) Derome, A. E. *Modern NMR Techniques of Chemistry Research*; Pergamon Press: Oxford, 1987; p 204.

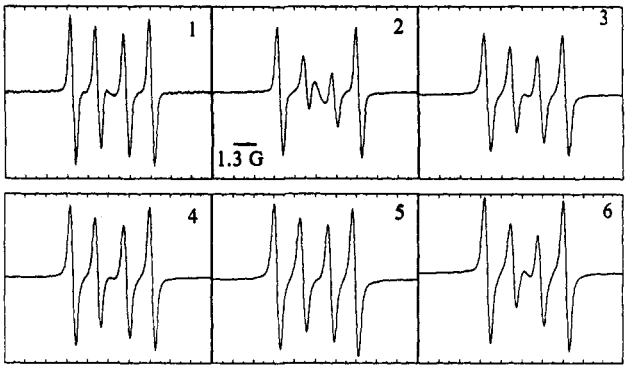

Figure 2. CW EPR spectra, recorded at RT, of solutions of $DtBPBQ^-$, Na^+ in THF with various concentrations: (1) 4.5×10^{-5} M; (2) 2.3×10^{-4} M; (3) 7.9×10^{-4} M; (4) 9.0×10^{-4} M; (5) 1.2×10^{-3} M; (6) 3.4×10^{-3} M.

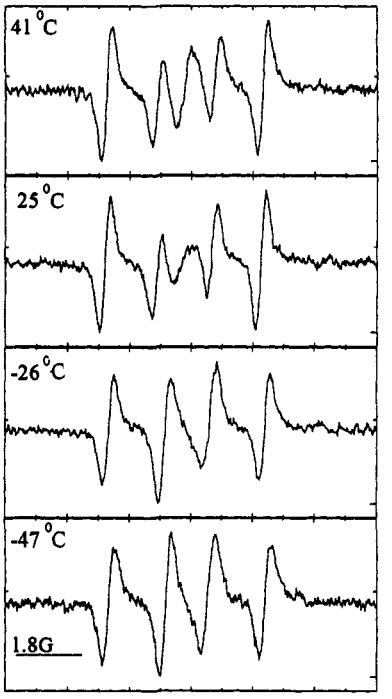

Figure 3. EPR spectra of $DtBPBQ^-$, Na^+ in THF (sample 2, 2.3×10^{-4} M) recorded at different temperatures, as indicated.

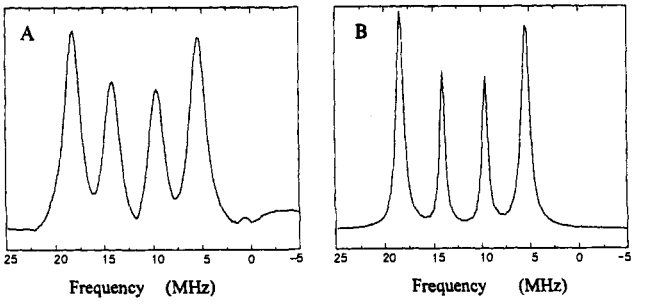

Figure 4. 1D FT-EPR spectra (RT) of solution 3; (A) magnitude spectrum; (B) real FT spectrum after reconstruction of the FID by linear prediction.

recorded with long τ_m required long acquisition times (several hours), during which some magnetic field drift of up to 100 mG was often observed, leading to some extra line broadening.

Data Manipulation. Prior to Fourier transformation zero filling to a 256 × 256 matrix was performed. In each dimension apodization with a sinbell function was performed. The overlap of the cross peaks with the tails of the intense diagonal peaks and the lower resolution of amplitude-mode spectra with respect to phase-sensitive spectra makes the determination of the volume integrals of the cross peaks difficult. We therefore

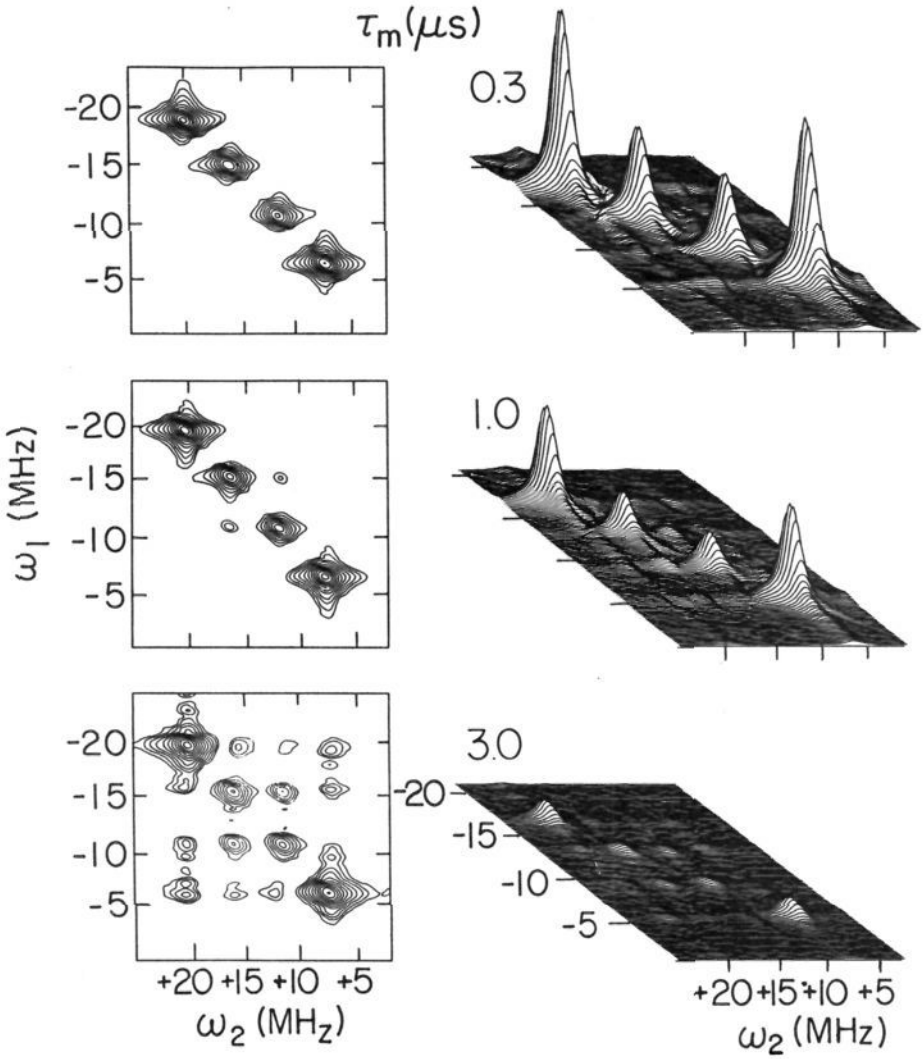

Figure 5. 2D exchange contour (left) and stack plot (right) spectra (RT) of DtBPBQ$^-$, Na$^+$ in THF, recorded with different mixing times, as indicated.

prefer to express the results in terms of peak amplitudes. When all peaks have similar widths, which well applies to our solutions, this introduces only a minor error.[9,27] The amplitudes of the peaks were determined as follows: cross sections along both ω_1 and ω_2 were taken for every diagonal peak, and the peak heights in the resulting 1D spectra were determined by applying proper base-line and peak overlaps corrections.

Results

1D CW and FT-EPR. The CW EPR spectra, recorded at RT, of the six samples under investigation are presented in Figure 2. All spectra show the expected four peaks (a doublet of doublets) with a_a = 1.5 G (4.20 MHz) and a_b = 3.1 G (8.68 MHz). The effect of increasing concentration on the line width, although small, is well noticeable. Comparison of the various spectra shows that the relative intensities of the inner two peaks vary from sample to sample, and often a rather broad center peak becomes apparent (see spectra of solutions 2, 3, and 6 in Figure 2). This indicates that the observed spectrum is a superposition due to two different ion-pairs of (DtBPBQ$^-$, Na$^+$), A and B. The spectrum of A, which is usually the major species, consists of four peaks with similar width, indicating that it is in the slow exchange regime. Ion-pair B exhibits two sharp peaks superimposed on the outer peaks of ion-pair A and two much broader inner peaks, which are usually too weak to observe. This species thus corresponds to an ion-pair undergoing fast intramolecular cation hopping.

The fast dynamics of ion-pair B becomes well evident when the spectra are recorded as a function of temperature. Figure 3 depicts the temperature dependence of the CW EPR spectrum of solution 3. At –47 °C both species are in the slow exchange region and the spectrum consists of four peaks with similar intensities. As the temperature is raised, the relative intensity of the inner peaks is reduced and eventually a broad center peak, generated by their coalescence, appears.

One-dimentional (1D) FT–EPR spectra of solution 3, measured at RT, is shown in Figure 4. Trace a shows a real (absorption mode) FT spectrum obtained after reconstruction of the FID by linear prediction (LP),[28] whereas trace b is a magnitude spectrum of the same raw data not treated with LP. Note that due to the dead time, the broad inner peaks of ion-pair B have disappeared in both spectra. Hence, the observed inner peaks are essentially due to ion-pair A alone, while the outer peaks correspond to both ion-pairs. We were unable to control the relative amounts of species A and B and so far did not find any correlation with the solutions' composition and/or the preparation conditions.

2D Exchange Results. Figure 5 shows 2D exchange spectra, displayed as contour and stack plots, of solution 3 recorded with mixing times of 0.3, 1.0, and 3.0 μs. To allow comparison of the absolute intensities, the stack plots were normalized to the strongest peak of the τ_m = 0.3 μs spectrum. The contour plots are not normalized; the lowest contour level in each spectrum

(27) Barsukov, I. L.; Pervishin, K. N.; Orekhov, V. Yu.; Barsukov, T. L.; Aiseniev, A. S. *Appl. Magn. Reson.* **1992**, *3*, 965.

(28) Barkhuijsen, H.; de Beer, R.; Bovee, W. M. M. J.; van Ormondt, D. *J. Magn. Reson.* **1985**, *61*, 465.

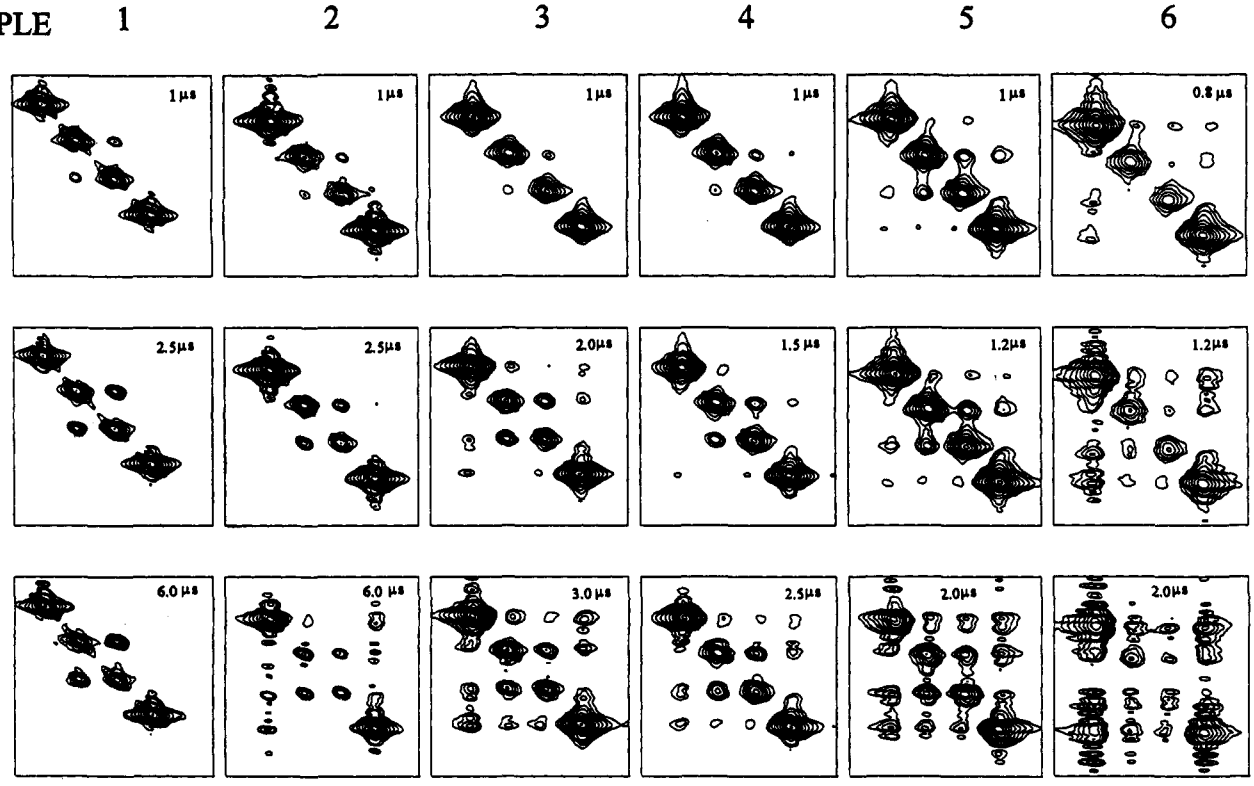

Figure 6. 2D FT-EPR exchange contour plot spectra of the various DtBPBQ$^-$, Na^+ solutions recorded at different mixing times, as indicated. Note that peaks in the spectra of solution 1 are slightly shifted as compared to the other spectra due to a somewhat different carrier frequency.

corresponds to a different amplitude. Note that as in the 1D case, the intensity of the outer peaks is greater than that of the inner ones due to the presence of species B. At short mixing times, $\tau_m = 0.3$ μs, the spectra display only diagonal peaks, whereas for $\tau_m = 1.0$ μs two cross peaks, generated by the CE, appear between the inner diagonal peaks. The spectra recorded with $\tau_m = 3.0$ μs exhibit cross peaks between all hyperfine lines, although those connecting the two inner peaks remain more intense than the others. At this mixing time the HE is no longer negligible and generates characteristic cross peaks of its own. The stack plots also illustrate the effect of T_1 relaxation, as manifested by the reduction of the overall signal intensity with increasing τ_m.

Figure 6 shows selected 2D spectra of the samples investigated at different mixing times. All samples exhibit the general trends presented in Figure 5 and in addition emphasize the increase in the HE rate with increasing ion-pair concentration. For instance, in sample 1 (4.5×10^{-5} M), the HE is negligible at $\tau_m = 2.5$ μs and only cross peaks due to CE are evident, whereas in sample 3 (7.9×10^{-4} M) the HE cross peaks are well evident at $\tau_m = 2.0$ μs, and for sample 6 (3.4×10^{-3} M) they show up already at $\tau_m = 0.8$ μs.

For convenience, in the ensuing discussion we labeled all peaks according to the inserted diagram in Figure 7 and divided them into four groups. Group a consists of the inner diagonal peaks 6 and 11, which are solely due to ion-pair A. Group b consists of the outer diagonal peaks, 1 and 16, to which both ion-pairs A and B contribute. Cross peaks 7 and 10 constitute group c, and their intensities, in dilute solutions, are primarily due to the CE in ion-pair A, whereas at high radical concentrations they are also affected by HE. All other cross peaks, 2, 3, 4, 5, 8, 9, 12, 13, 14, and 15, which are comprised in group d are, to first order in τ_m, generated by pure HE. With increasing mixing times, second- and third-order exchange effects become effective and the distinction between "pure" HE and CE peaks is no longer applicable. For the presentation of the results we define the average peak intensity, I_i of group i, as the total peak intensity of the group divided by the number of peaks in it. Figure 7 shows the τ_m dependence of the average peak intensities, for the various samples studied. In all plots they are normalized with respect to I_a at the shortest mixing time, $\tau_m = 0.3$ μs. Note that I_d, which is the smallest of all, is multiplied by a factor of 5. In all cases the intensities of the diagonal peaks, I_a and I_b, decay monotonically with τ_m due to the T_1 and exchange processes, while the cross peak intensity I_c first increases with τ_m, as expected for CE, and then decreases due to relaxation effects.[21] In principle, I_d should have the same general behavior as I_c, except for a shift in the position of the maximum due to the different rates of the HE. In practice however, the experimental points of I_d are more scattered because the HE cross peaks are generally much weaker compared to those of CE. Therefore, in the final quantitative analysis, to be presented below, we gave I_d less weight.

Determination of the Rate Parameters. In order to determine the CE, HE, and T_1 relaxation rates, the exchange matrix **R** has to be defined (eq 2). Its entries have contributions from both ion-pairs A and B, since they are coupled by collisions which contribute to the HE cross peaks (group d). Accordingly, the dimension of the exchange matrix is 8×8, as given in Table 4. It includes the relaxation times T_1(A) and T_1(B) of species A and B, the CE rate of A, K_{CE}^A, and four HE rates, K_{AA}, K_{AB}, K_{BA}, and K_{BB}, due to pairwise collisions of the ion-pairs. We omitted the CE rate of ion-pair B because, as already discussed, at RT it is relatively fast and results in excessive broadening of its two inner peaks, which are eliminated from the FT-EPR spectrum due to the spectrometer dead time. In the calculations, these peaks were "removed" by associating with them a very short (0.04 μs) phenological "T_2" as compared to $T_2 = 0.84$ μs for all other peaks. This procedure also leads to a reduction in the intensity of cross peaks 2, 3, 8, 12, 15, 14, 9, and 5 with respect to peaks 4 and 13, as in fact observed in the experiment. The relative amounts of A and B are taken into account in the corresponding $P_j(0)$s (eq 2).

To facilitate the quantitative analysis, we first estimated T_1(A) and T_1(B) for each solution by following the decay of the total signal, given by the sum of all the peak amplitudes. The

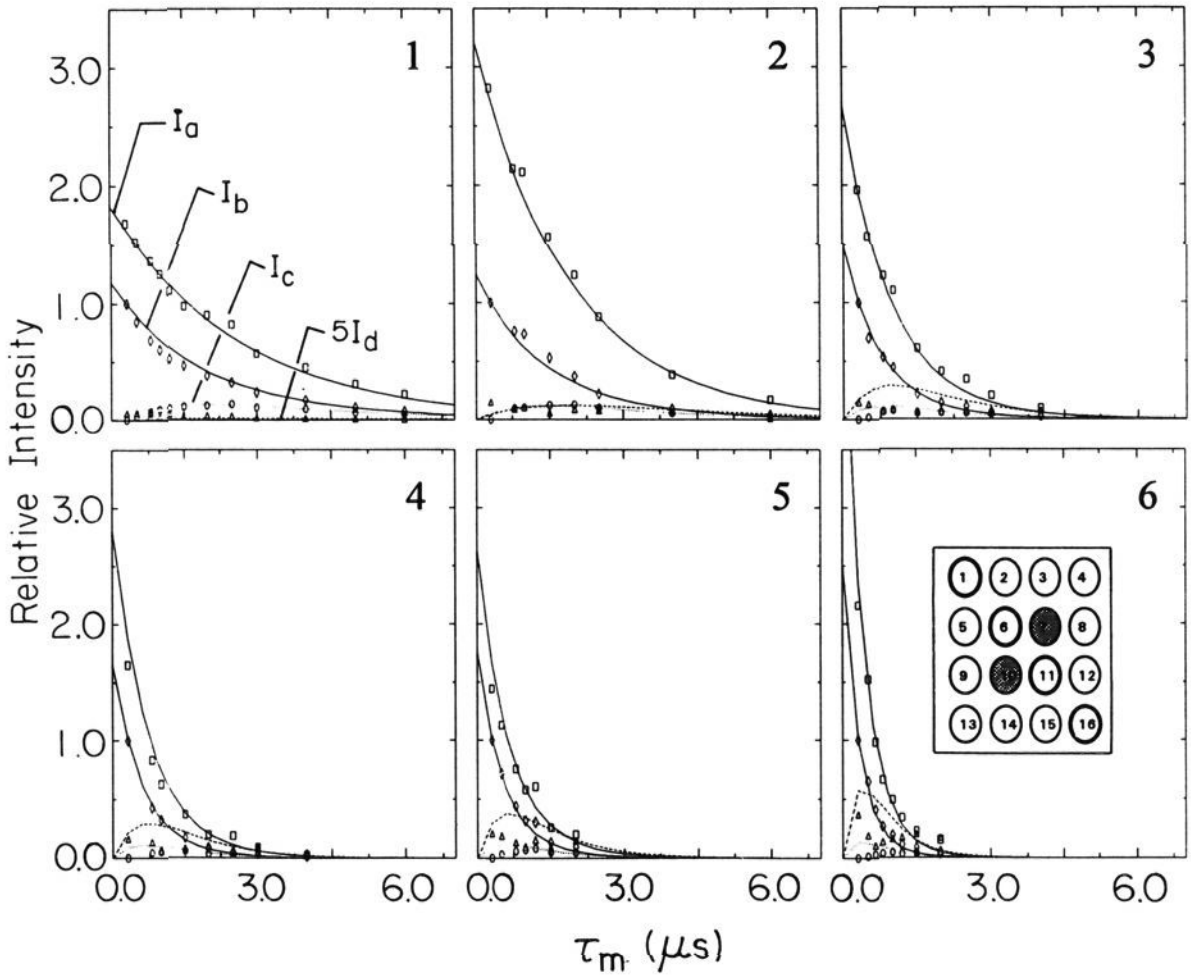

Figure 7. Plots of the group intensities, I_a–I_d, of samples 1–6 as a function of τ_m. The points are experimental, and the curves are from a simulation (eq 2) obtained with the parameters listed in Table 3. The line widths used were 0.25 G for all outer peaks and the inner peaks of A and 5 G for the inner peaks of B. The inserted diagram shows the peaks' labeling.

Table 3. Summary of the Exchange Rates and Relaxation Times for the Samples Studied[a]

sample no.	DtBPBQ (M)	[A]	[B]	[B]/[A][a]	K_{AA} (10^6 s^{-1})	K_{BB} (10^6 s^{-1})	T_1 [b] (μs)	T_1 [c] (μs)
1	4.5×10^{-5}	2.9×10^{-5}	1.6×10^{-5}	0.55	0.01	0	2.7	2.7
2	2.3×10^{-4}	8.6×10^{-5}	1.4×10^{-4}	1.6	0.07	0.02	2.1	2.1
3	7.9×10^{-4}	4.4×10^{-4}	3.5×10^{-4}	0.8	0.4	0.03	1.2	1.6
4	9.0×10^{-4}	5.3×10^{-4}	3.7×10^{-4}	0.7	0.5	0.03	0.9	0.8
5	1.2×10^{-3}	8.3×10^{-4}	4.1×10^{-4}	0.5	0.6	0.07	0.8	0.9
6	3.4×10^{-3}	1.7×10^{-3}	1.7×10^{-3}	1	1.1	0.15	0.5	0.5

[a] $K_{CE}^A = (1.7 \pm 0.2) \times 10^5$ s^{-1}. [b] The value from the 2D simulation. [c] The value from the decay of the sum of all signals of the 2D spectra.

results are shown in Figure 8. They could well be fitted to a single decaying exponent, and the values obtained are listed in Table 3. The observation of a single exponent indicates that $T_1(A) \approx T_1(B)$. We note, however, that with the quality of our data we cannot rule out a factor of ~2 between the two relaxation times. We also used the values of I_a and I_c in the more dilute solutions, where the HE is negligible, to estimate T_1 (A) and K_{CE}^A by employing eq 3. With these results we calculated the initial amplitudes of the outer diagonal peaks of ion-pair A and by comparison with the amplitudes of the outer peaks in the experimental spectra derived the relative amount of species B and $T_1(B)$. Within the experimental accuracy we found again that $T_1(A) \approx T_1(B) = T_1$ in all samples. The relative amounts of A and B obtained in this way are given in Table 3. They are generally in reasonable (±50%) agreement with those obtained by the direct measurement of the relative intensities of the inner and outer peaks in the one-dimensional FT and CW EPR spectra. The actual values used in the analysis (as given in Table 3) are those determined by the 2D data. We chose this set because their derivation inherently includes corrections due to possible differences in the T_1 relaxation. The initial estimates of T_1 and K_{CE}^A served as starting values in the final fit of all the experimental 2D spectra in which also the various HE rate constants were included. In this procedure we compared the calculated 2D spectra with the experimental ones and readjusted all parameters until a best visual fit was obtained.

Due to experimental errors and the limited number of data points for each solution, we tried to minimize the number of parameters to be fitted. We first assumed that the HE rate constants are similar for all possible exchange processes, namely, $K_{AA} = K_{BA} = k[A]$ and $K_{AB} = K_{BB} = k[B]$. This assumption was found not valid. In particular the relative amplitudes of the HE cross peaks 4 and 13 compared to the other peaks in group d did not conform with the experiments. When the relative intensity of the former was right, that of the latter was too low and vice versa. This indicates that the HE rate constants are not all equal and that those related to ion-pair B are probably lower.

Next we set the HE rate constants determining the AA

Table 4. The Exchange Matrix

	$\alpha_A\alpha_A$	$\alpha_A\beta_A$	$\beta_A\alpha_A$	$\beta_A\beta_A$	$\alpha_B\alpha_B$	$\alpha_B\beta_B$	$\beta_B\alpha_B$	$\beta_B\beta_B$
$\alpha_A\alpha_A$	$-{}^3/_4K_{AA} - 1/T_1 - K_{AB}$	${}^1/_4K_{AA}$	${}^1/_4K_{AA}$	${}^1/_4K_{AA}$	${}^1/_4K_{AB}$	${}^1/_4K_{AB}$	${}^1/_4K_{AB}$	${}^1/_4K_{AB}$
$\alpha_A\beta_A$	${}^1/_4K_{AA}$	$-K^A_{CE} - {}^3/_4K_{AA} - 1/T_1 - K_{AB}$	$K^A_{CE} + {}^1/_4K_{AA}$	${}^1/_4K_{AA}$	${}^1/_4K_{AB}$	${}^1/_4K_{AB}$	${}^1/_4K_{AB}$	${}^1/_4K_{AB}$
$\beta_A\alpha_A$	${}^1/_4K_{AA}$	$K^A_{CE} + {}^1/_4K_{AA}$	$-K^A_{CE} - {}^3/_4K_{AA} - 1/T_1 - K_{AB}$	${}^1/_4K_{AA}$	${}^1/_4K_{AB}$	${}^1/_4K_{AB}$	${}^1/_4K_{AB}$	${}^1/_4K_{AB}$
$\beta_A\beta_A$	${}^1/_4K_{AA}$	${}^1/_4K_{AA}$	${}^1/_4K_{AA}$	$-{}^3/_4K_{AA} - 1/T_1 - K_{AB}$	${}^1/_4K_{AB}$	${}^1/_4K_{AB}$	${}^1/_4K_{AB}$	${}^1/_4K_{AB}$
$\alpha_B\alpha_B$	${}^1/_4K_{BA}$	${}^1/_4K_{BA}$	${}^1/_4K_{BA}$	${}^1/_4K_{BA}$	$-{}^3/_4K_{BB} - 1/T_1 - K_{BA}$	${}^1/_4K_{BB}$	${}^1/_4K_{BB}$	${}^1/_4K_{BB}$
$\alpha_B\beta_B$	${}^1/_4K_{BA}$	${}^1/_4K_{BA}$	${}^1/_4K_{BA}$	${}^1/_4K_{BA}$	${}^1/_4K_{BB}$	$-{}^3/_4K_{BB} - 1/T_1 - K_{BA}$	${}^1/_4K_{BB}$	${}^1/_4K_{BB}$
$\beta_B\alpha_B$	${}^1/_4K_{BA}$	${}^1/_4K_{BA}$	${}^1/_4K_{BA}$	${}^1/_4K_{BA}$	${}^1/_4K_{BB}$	${}^1/_4K_{BB}$	$-{}^3/_4K_{BB} - 1/T_1 - K_{BA}$	${}^1/_4K_{BB}$
$\beta_B\beta_B$	${}^1/_4K_{BA}$	${}^1/_4K_{BA}$	${}^1/_4K_{BA}$	${}^1/_4K_{BA}$	${}^1/_4K_{BB}$	${}^1/_4K_{BB}$	${}^1/_4K_{BB}$	$-{}^3/_4K_{BB} - 1/T_1 - K_{BA}$

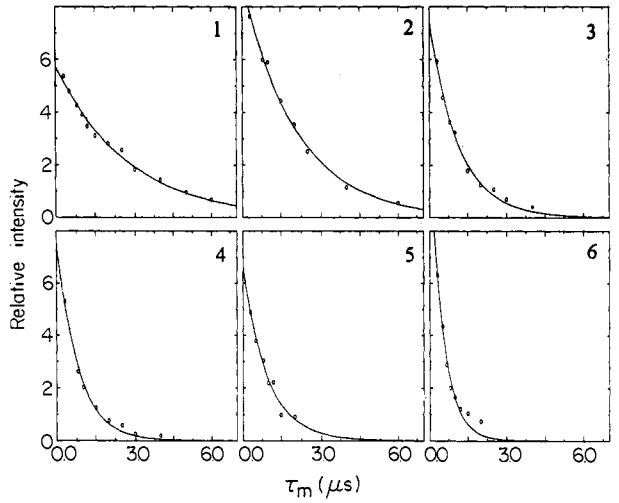

Figure 8. Plots of the sum of all peak intensities in the 2D spectra for each sample (1–6) as a function of τ_m. The solid curves were calculated with $e^{-\tau_m/T_1}$ with the T_1 values given in Table 3.

exchange to be k_A and that of BB to be k_B, and we assumed that all the other rate constants that involve species B are equal to the latter, namely, $k_{AB} = k_{BA} = k_{BB} = k_B$. This resulted in a significantly improved agreement with the experimental results. The parameters so obtained (see Table 3) were used to calculate the 2D maps of Figure 9 as well as the intensity curves in Figure 7. Note the somewhat shorter T_1 (0.5 μs) compared the assumed T_2 (0.84 μs) in solution 6, which must be ascribed to a best fit artifact. The difference is certainly within our experimental accuracy and indicates that at high radical concentrations the line width is T_1 limited. The dependence of K_{AA} and K^A_{CE} on [A] and of K_{BB} on [B] is shown in Figure 10. As expected, K^A_{CE} is independent of the concentration, while both K_{AA} and K_{BB} increase linearly with the radical concentration, yielding $k_A = (7.5 \pm 1.0) \times 10^8$ s^{-1} mol^{-1} and $k_B = (1.0 \pm 0.2) \times 10^8$ s^{-1} mol^{-1}.

Discussion

Two significantly different rates for the Na$^+$ hopping in DtBPBQ$^-$, Na$^+$ ion pairs in THF at 20 °C have been reported, one by Hirota and co-workers[2] (1.5×10^5 s^{-1}) and the other by Warhurst and co-workers[17] (3.4×10^4 s^{-1}).[17] Our result ((1.7 ± 0.2) $\times 10^5$ s^{-1}) agrees well with the results of Hirota and co-workers.[2] The rate constant for the HE due to collisions between these ion-pairs ($k_A = (7.5 \pm 1.0) \times 10^8$ s^{-1} mol^{-1}) is significantly lower than corresponding values determined for neutral radicals[29,30] in similar solvents ($\sim 5 \times 10^9$ s^{-1} mol^{-1}).[32] It is also lower than those measured for electrochemically generated duroquinone (DQ)((2.98 ± 0.2) $\times 10^9$ s^{-1} mol^{-1}) and parabenzoquinone (PBZQ) ((3.52 ± 0.12) $\times 10^9$ s^{-1} mol^{-1}) anion radicals in dimethoxyethane (DME) at 15 °C.[31] Our value, however, is similar to that found in the (tetracyanoethylene$^-$, Li$^+$) ion-pair.[32]

An extensive theory for the spin exchange frequency in solutions of free radicals was developed by Freed and co-workers.[30,33] In addition to the hydrodynamic properties of the solution the theory takes into account the interaction potential of the colliding radicals and the detailed nature of the exchange interaction. In a simplified form the rate constant for the exchange can be written as[29,34]

$$k_e = (8/3)pfkT/\eta \qquad (4)$$

where η is the viscosity, f is a steric factor depending on the shape, the interaction potential, and the exchange interaction of the colliding radicals, and p is the average efficiency of the spin exchange for a collision. For the case of spin 1/2

$$p = \frac{1}{2}\frac{J^2\tau_c^2}{1 + J^2\tau_c^2} \qquad (5)$$

where J is the average exchange energy during a collision and τ_c is the duration of a collision. In the strong exchange limit, $J^2\tau_c^2 \gg 1$, $k_e = (4/3)fkT/\eta$; that is, for each collision there is 50% chance of spin exchange, whereas in the case of weak exchange, $J^2\tau_c^2 \ll 1$, $k_e = (4/3)J^2\tau_c^2 fkT/\eta$; the probability for spin exchange is proportional to $(J\tau_c)^2$. For the strong exchange limit, taking $f = 1$ and $\eta = 0.5$ cP, eq 4 predicts $k_e \approx 6.5 \times 10^9$ s^{-1} mol^{-1},[30] as compared to our experimental result of $k_A = (7.5 \pm 1.0) \times 10^8$ s^{-1} mol^{-1}. The discrepancy may be accounted for by assuming a steric factor of $f \sim 0.1$, which is not unreasonable for the DtBPBQ$^-$, Na$^+$ ion-pairs. These ion-pairs are far from being spherical, and the spin exchange probability is probably highly anisotropic, as it depends on the spin density distribution in the ion-pair. Moreover, effects of charge distribution and interaction potential between the colliding species may also be important, as they are ion-pairs rather than neutral molecules. A similar explanation was given to the reduced HE rate constant of DQ

(29) Molin, Yu. N.; Salikhov, K. M.; Zamaraev, K. I. *Spin Exchange; Principles and Applications in Chemistry and Biology*; Springer Series in Chemical Physics 8; Springer-Verlag: New York, 1980.
(30) Eastman, M. P.; Kooser, R. G.; Das, M. R.; Freed, J. H. *J. Chem. Phys.* **1969**, *51*, 2690.
(31) Leniart, D. S.; Connor, H. D.; Freed, J. H. *J. Chem. Phys.* **1975**, *63*, 165.
(32) Komarinsky, M. A.; Wahl, A. C. *J. Phys. Chem.* **1975**, *79*, 695.
(33) Freed, J. H.; Pedersen, J. B. *Adv. Magn. Reson.* **1976**, *8*, 1.
(34) Nayeerm, A.; Rananavare, S. B.; Sastry, V. S. S.; Freed, J. H. *J. Chem. Phys.* **1989**, *91*, 6887.

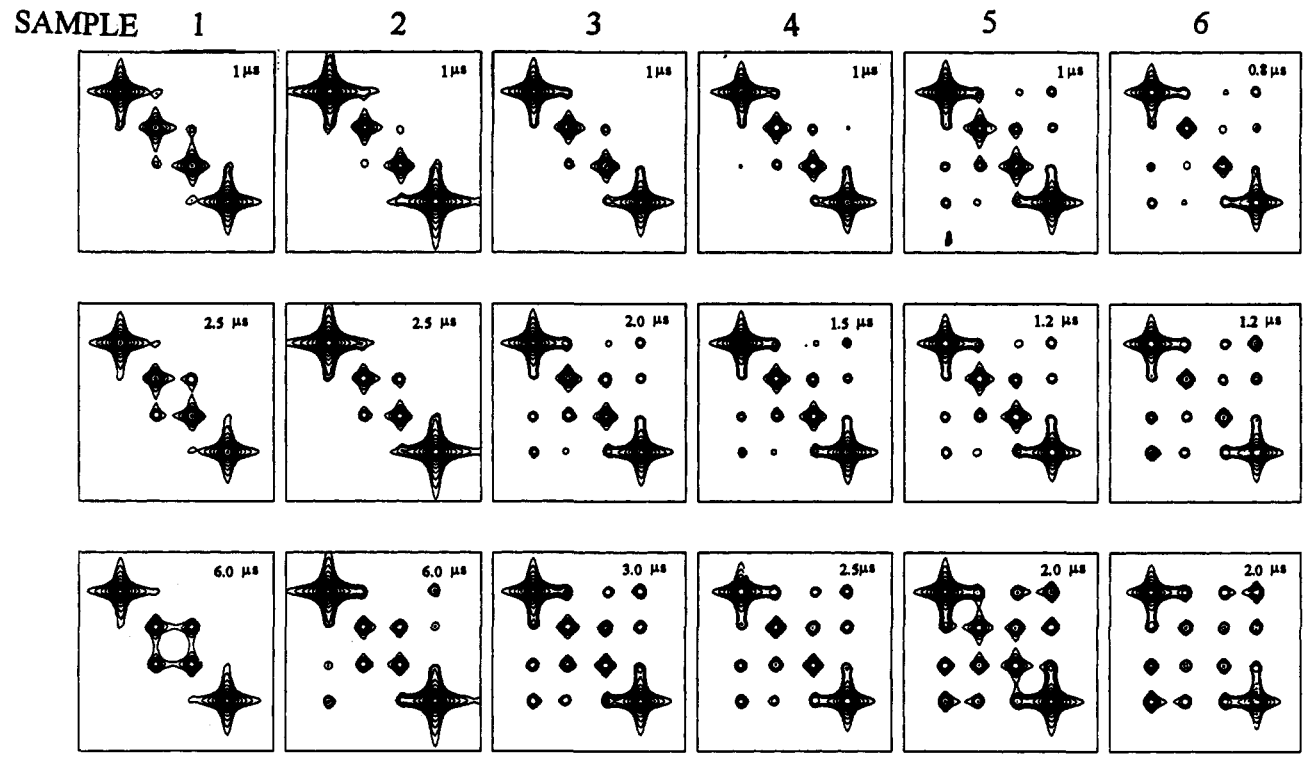

Figure 9. Simulated 2D maps of samples 1–6 to be compared with Figure 6. The parameters used in the simulations are given in Table 3, and the line widths used are as in Figure 7.

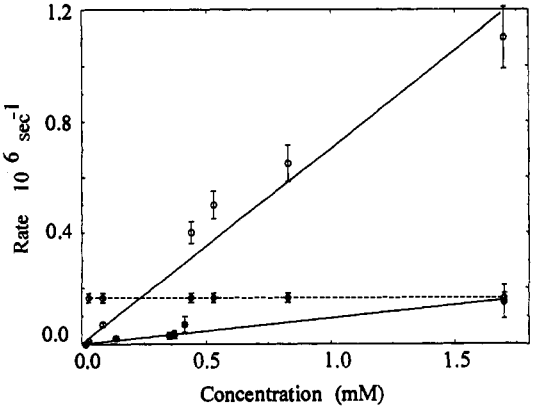

Figure 10. Dependence of K_{CE}^{A} (□) and K_{AA} (○) on [A] and of K_{BB} (●) on [B].

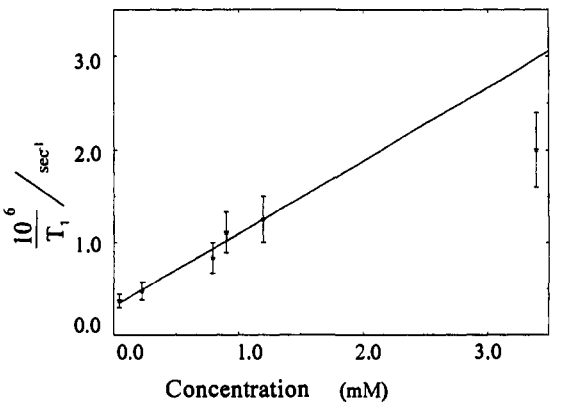

Figure 11. Plot of the experimental $1/T_1$ against the overall radical concentration. The linear fit corresponds to $1/T_1 = (0.3 \pm 0.3) \times 10^6 + (7.8 \pm 0.8) \times 10^8$[M].

radical anion in DME.[35] Alternatively the low value of k_A can, at least partially, be due to weak exchange with $0.1 < (J\tau_c)^2 < 1$. A distinction between the two effects can in principle be made by determining the dependence of k_A on the viscosity of the solvent. For weak exchange k_e increases with η, whereas for strong exchange the opposite is expected.[29]

The experiments also provide the decay rates, $1/T_1$, of the overall magnetization in the various solutions (Table 3). These were found to be similar for the two radicals and to increase monotonically with the radical concentration. The experimental results are plotted in Figure 11 as a function of the total radical concentration, where it may be seen that the dependence is nearly linear:

$$\frac{1}{T_1} = a + b[\mathrm{M}] \qquad (6)$$

with $a = (0.3 \pm 0.3) \times 10^6\ \mathrm{s^{-1}}$ and $b = (7.8 \pm 0.8) \times 10^8\ \mathrm{s^{-1}\ mol^{-1}}$. The mechanism of this relaxation process cannot be the HE which results in interchange between spin polarizations, whereas the T_1 process corresponds to the decay of the overall magnetization. The concentration dependent part of this relaxation is most likely due to electron–electron dipolar interaction between pairs of colliding radicals. For a very rough estimate of this effect we can use the point dipole model and follow Abragam's derivation for the corresponding mechanism in NMR.[36] In the extreme narrowing limit and using the Stokes–Einstein approximation for the self-diffusion, the electron–electron dipolar contribution to the longitudinal relaxation (in $\mathrm{s^{-1}}$) becomes

$$\left(\frac{1}{T_1}\right)_{dd} = \frac{6\pi^2\gamma^4\hbar^2\eta A_v}{5 \times 10^3\, kT}[\mathrm{M}] \qquad (7)$$

where A_v is Avogadro's number and the constants are in centimeter-gram-second units. Inserting the appropriate values in eq 7 yields $(1/T_1)_{dd} = 0.16 \times 10^8$[M] $\mathrm{s^{-1}}$. This value is about a factor of 50 smaller than the experimental result of 7.8×10^8-

(35) Eastman, M. P.; Bruno, G. V.; Freed, J. H. *J. Chem. Phys.* **1970**, *52*, 2511.

(36) Abragam, A. *The Principles of Nuclear Magnetism*; Oxford University Press, London, 1961; Chapter 8.

$[M]\ s^{-1}$. The discrepancy is at least partly due to the inapplicability of the point dipole approximation for the interaction between electrons. This approximation will generally yield low values than in reality. Other contributions to the discrepancy may originate from the fact that the radicals are not neutral hard spheres and perhaps that the extreme narrowing condition is not completely fulfilled. In fact, considering the crudeness of the model, the discrepancy between the experimental result and the prediction of eq 7 is not that large.

Finally we discuss the nature and possible structures of the second ion-pair, B. Although there have not been specific reports regarding the existence of two types of ion-pairs of $DtBPBQ^-$, Na^+ in THF, the concept that several different ion-pairs as well as the free ion radical can coexist at equilibrium is well documented in the literature.[1] For example, certain types of ion-pairs have been referred to as "tight" or "contact" ion-pairs, in which alkali metal hyperfine splittings are observed, while others were termed "loose" or "solvent-separated" ion-pairs, when no such splittings were detected.[1,37,38] We already excluded the possibility that B is the free anion radical because of its temperature dependent EPR spectrum (Figure 3). The appearance of a superposition of the spectra due to species A and B up to 50 °C indicates that within the temperature range investigated the interconversion between them is slow on the EPR time scale. Interconversion between A and B could in principle be studied by 2D exchange experiments at temperatures where the intramolecular cation jump in B has reached the fast limit (~50 °C). In this case additional cross peaks between the center peak of B and the two inner peaks of A would be the signature of the A ⇄ B process.

The conditions under which species B is formed remain unclear. We found no correlation with the concentration of the quinone or with any other parameter related to the preparation procedure. We therefore infer that it must be related to some kind of "impurity". One possibility could be potassium ions from the glass surface or from the metallic sodium leading to the formation of $DtBPBQ^-$, K^+.[39] The latter undergoes faster cation hopping than the corresponding Na^+ ion-pair.[17] In this case however we would expect a reduction in the relative amount of B with increasing quinone concentration because the same reaction apparatus was used for all preparations. Such a trend has not been observed, and we therefore exclude this possibility.

Another possible impurity is traces of water in the THF. This impurity is known to produce the free anion radical,[40] which was not observed in our spectra. It is also unlikely that traces of water still exist in our solutions, which were prepared with a large excess of sodium. Any water present would react to yield OH^-, H_2, and Na^+, thus generating excess Na^+ relative to the anion

Scheme 2

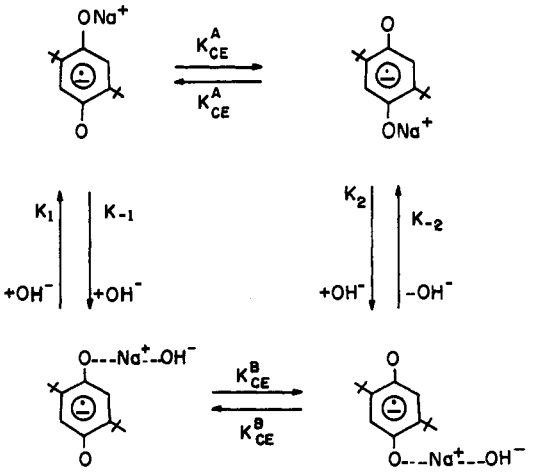

radical, which would merely enhance the apparent cation hopping in ion-pair A due to intermolecular cation exchange.[41] However, for a significant increase in the hopping rate a relatively large excess of Na^+(0.02 M) would be required.

A plausible structure of ion-pair B is that of an ion-pair with OH^- ions associated in the solvation shell of the cation. It has been found[42] that 2-propanol enhances the intramolecular cation hopping in THF solutions of $DtBPBQ^-$, Na^+, and it is possible that OH^- ions formed by traces of water may have a similar effect. Small amounts of OH^- ions will transform part of the ion-pairs A to the OH^--associated ion-pair B. Since the samples were prepared at different times, the water content of the solvent may have been different, leading to different concentrations of B. Accordingly, we propose the model shown in Scheme 2 for the chemical exchange processes taking place in the system investigated with $K^A_{CE} < K^B_{CE}$ and $k_1, k_{-1}, k_2, k_{-2} \ll K^A_{CE}$. The complex structure for species B is also consistent with its lower HE rate, as the different charge distribution may lead to a lower steric factor.

Conclusions

2D FT-EPR exchange spectroscopy is a powerful method for studying slow chemical exchange processes in solutions of radicals. It can be used to study reaction mechanism and for quantitative determination of the exchange rates in the presence of a complex array of dynamic processes.

Acknowledgment. This study was made possible by Grant 90-00128 from the United States–Israel Binational Science Foundation, Jerusalem. We thank M. K. Bowman for many helpful discussions. We also thank H. Zimmermann for his continuous help.

(37) Hirota, N. *J. Am. Chem. Soc.* **1968**, *90*, 3603.
(38) Khakhar, M. P.; Prabhananda, B. S.; Bas, M. R. *J. Chem. Phys.* **1966**, *45*, 2327.
(39) Graceffa, P.; Tuttle, T. R. *J. Chem. Phys.* **1969**, *50*, 1908.
(40) Lucken, E. A. *J. Chem. Soc., Faraday Trans.* **1964**, 4234.
(41) Rutter, A. W.; Warhurst, E. *Trans. Faraday Soc.* **1968**, *64*, 2338.
(42) Chen, K. S.; Hirota, N. *J. Phys. Chem.* **1978**, *82*, 1133.